21 June 2001

PHYSICS LETTERS B

ELSEVIER

Physics Letters B 510 (2001) 17–23

www.elsevier.nl/locate/npe

New evidence for a subshell gap at $N = 32$

J.I. Prisciandaro [a,b], P.F. Mantica [a,b], B.A. Brown [a,c], D.W. Anthony [a,b], M.W. Cooper [d], A. Garcia [e], D.E. Groh [a,b], A. Komives [e], W. Kumarasiri [a,b], P.A. Lofy [a,b], A.M. Oros-Peusquens [b], S.L. Tabor [d], M. Wiedeking [d]

[a] *Department of Chemistry, Michigan State University, East Lansing, MI 48824, USA*
[b] *National Superconducting Cyclotron Laboratory, Michigan State University, East Lansing, MI 48824, USA*
[c] *Department of Physics and Astronomy, Michigan State University, East Lansing, MI 48824, USA*
[d] *Department of Physics, Florida State University, Tallahassee, FL 32306, USA*
[e] *Department of Physics, University of Notre Dame, Notre Dame, IN 46556, USA*

Received 28 March 2001; received in revised form 24 April 2001; accepted 1 May 2001
Editor: J.P. Schiffer

Abstract

An 879.9(2) keV γ-ray transition has been identified following the β decay of ^{58}V and assigned as the $2_1^+ \rightarrow 0_1^+$ transition in $^{58}Cr_{34}$. A peak in the energies of the first excited 2^+ states for the even–even chromium isotopes is now evident at $^{56}Cr_{32}$, providing empirical evidence for a significant subshell gap at $N = 32$. The appearance of this neutron subshell closure for neutron-rich nuclides may be attributed to the diminished $\pi 1f_{7/2}$–$\nu 1f_{5/2}$ monopole proton–neutron interaction as protons are removed from the $1f_{7/2}$ single-particle orbital. © 2001 Elsevier Science B.V. All rights reserved.

PACS: 21.60.Cs; 23.20.Lv; 27.40.+z

Trends in nuclear masses and binding energies have suggested nuclei associated with nucleon numbers 2, 8, 20, 28, 50, 82 and 126 exhibit an extra degree of binding. The existence of these magic numbers was one of the empirical evidences for the development of the nuclear shell model [1]. Macroscopically, nuclei with protons or neutrons filling a magic shell may be described with spherical charge distributions and modest collective features at low excitation energy. Between the magic shell closures, collective interactions amid nucleons becomes evident, in the form of vibrational and rotational excitations within their low-energy level spectrum. These collective excitations are expected to be maximum at midshell. However, the development of collectivity away from major closed shells may be inhibited by the presence of subshell closures, or minor shell gaps.

In order to study such phenomena, experimental probes of quadrupole collectivity may be utilized. One measure of the extent of quadrupole collectivity in even–even nuclear systems is the energy of the first excited 2^+ state, $E(2_1^+)$. According to Grodzins [2,3], $E(2_1^+)$ is inversely proportional to the quadrupole deformation parameter, β_2. Thus, near-spherical nuclei will exhibit high $E(2_1^+)$ values relative to neighboring even–even isotopes. As nucleons are added to the system, $E(2_1^+)$ will decrease, a result of the dominance of collective interactions amongst nucleons. The existence of subshells between major shell closures should

E-mail address: prisc@nscl.msu.edu (J.I. Prisciandaro).

0370-2693/01/$ – see front matter
PII: S0370-2693(01)00565-2

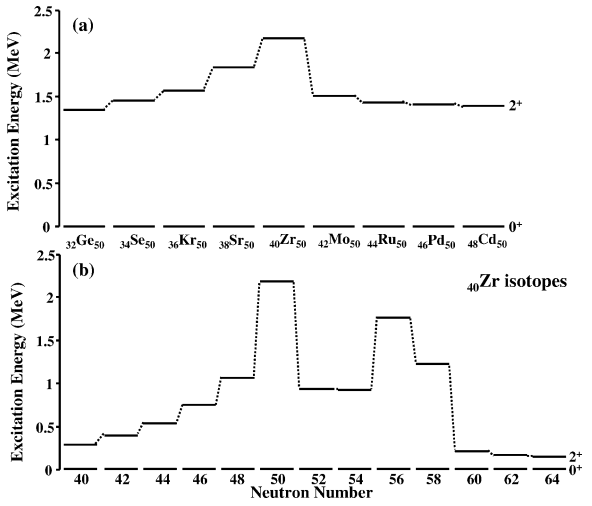

Fig. 1. $E(2_1^+)$ systematics for (a) even–even $N = 50$ isotones and (b) neutron-rich zirconium isotopes. The $E(2_1^+)$ values for Ge to Pd were obtained from Ref. [4] and Cd from Ref. [5].

result in similar $E(2_1^+)$ trends. As an example, the $E(2_1^+)$ systematics for even–even $N = 50$ isotones are shown in Fig. 1a. The depicted $E(2_1^+)$ values were obtained from Refs. [4,5]. Although the major proton shell spans from $Z = 28$–50, there is a clear increase in $E(2_1^+)$ at ^{90}Zr, $Z = 40$. This rise in $E(2_1^+)$ suggests a substantial energy gap between the $\pi 2p_{1/2}$ and $\pi 1g_{9/2}$ single-particle orbitals. An inspection of the $E(2_1^+)$ values for neutron-rich, even–even zirconium isotopes reveals a similar peak at $N = 56$ (see Fig. 1b). Sadler et al. [6] have suggested that the significant energy gap between the $\nu 2d_{5/2}$ and the $\nu 1g_{7/2}$ orbitals may be attributed to the $N = 56$ subshell.

Based on self-consistent energy density calculations, Tondeur [7] proposed $N = 32$ as a new magic number for neutron-rich nuclides. Following the beta decay of ^{52}K, Huck et al. [8] assigned the 2.56 MeV state in $^{52}_{20}\mathrm{Ca}_{32}$ a spin and parity of 2^+. As compared to the first excited 2^+ level in ^{50}Ca, an increase in $E(2_1^+)$ was observed. Based on this finding, Huck et al. [8] suggested the rise at $N = 32$ was due to the $\nu 2p_{3/2}$ subshell closure, indicating that $N = 32$ was semi-magic. This assertion was consistent with Tondeur's theoretical prediction [7]. Following a mass measurement of ^{52}Ca [9], an increase in binding was also noted at $N = 32$. However, when considering the rise in $E(2_1^+)$ for ^{52}Ca, one must bear in mind the uncertainty associated with the spin and parity assignment of this state. In addition, in the absence of mass measurements for ^{54}Ca and more neutron-rich calcium isotopes, the systematics of pairing energy and two-neutron separations are inconclusive. Using a shell-model calculation, Richter et al. [10] predicted the first excited 2^+ state of ^{52}Ca at 1.85 MeV. Recalculating the single-particle energies of this nuclide based on a shell model plus Hartree–Fock approximation [11], the 2_1^+ state was predicted at 1.91 MeV. Both of these theoretical values are significantly lower than the "suggested" experimental value. Based on this finding, the authors attributed the rise in $E(2_1^+)$ to the filling of the $\nu 2p_{3/2}$ subshell, suggesting $N = 32$ is a good subshell closure for calcium.

The motivation for this study was to explore the mass region $A = 50$–60 to confirm the $N = 32$ subshell closure for neutron-rich nuclides. The extension of the $E(2_1^+)$ systematics to heavier calcium isotopes would be of value, however, at present these nuclei are difficult to produce with sufficient statistics. Therefore, for this study, the systematics of the chromium isotopes were examined. Similar to the case of $^{52}_{20}\mathrm{Ca}_{32}$, the first 2^+ state of $^{56}_{24}\mathrm{Cr}_{32}$ lies higher in energy relative to its $N - 2$ neighbor, $^{54}\mathrm{Cr}_{30}$. However, unlike $^{52}\mathrm{Ca}_{32}$, the spin and parity assignment of the 2^+ level for $^{56}\mathrm{Cr}_{32}$ was deduced from the shape of proton angular distribution curves following its production via the (t, p) reaction [12]. A second (t, p) study confirmed the spin-parity assignments for a number of states, including the first excited 2^+ state at 1007 keV [13]. The authors also reported that shell model calculations reproduced the energy of the first excited 2^+ state. To determine whether the first excited 2^+ energies continued to rise or peaked at $N = 32$, it was necessary to measure $E(2_1^+)$ beyond $N = 32$. In this Letter, the energy of the first excited 2^+ state of ^{58}Cr is presented. A preliminary report is given in Ref. [14].

In order to study the low-energy properties of ^{58}Cr, the parent nuclide, ^{58}V, along with several other neutron-rich nuclides were produced via projectile fragmentation of a 70 MeV/nucleon ^{70}Zn beam in a ^{9}Be target at the National Superconducting Cyclotron Laboratory at Michigan State University. The fragments of interest were separated from other reaction products using the A1200 fragment analyzer. Further separation was achieved by passing the radioactive

beam through the Reaction Products Mass Separator (RPMS). To monitor the beta activity, a double-sided Si strip detector (DSSD) segmented into 40 1 mm wide strips in x and y dimensions was utilized. A 985 μm thick DSSD was selected to ensure sufficient Si for the detection of high-energy beta particles expected from the decay of nuclei far removed from the line of β stability. The DSSD was positioned between two 5 cm $\times$ 5 cm Si PIN detectors, placed at distances 1.9 cm and 2.2 cm, respectively, from the center of the DSSD. The upstream PIN detector had a thickness of 309 μm, while the downstream detector was 503 μm thick. Further upstream from the PIN-DSSD-PIN detector telescope was a 300 μm Si PIN detector. This PIN detector provided energy loss and, in conjunction with the cyclotron frequency, time of flight (TOF) for particle identification.

Beta activity from the implanted ions was confirmed with the coincidence of low-energy events within the DSSD and one of the Si PIN detectors located on either side of the DSSD. Due to the relatively long half-lives associated with beta decay, it was important to maintain an implantation rate that allowed sufficient time between implants to cleanly correlate implants with successive beta decay events. On average, ions were implanted into the strip detector at a rate no greater than 100 s^{-1}. The beam was defocused in both x and y to illuminate $\approx 2/3$ of the active detector area. This beam profile resulted in an average two-second time window between successive implants in the central most portion of the DSSD. This provided ample time for measuring the half-lives of the short-lived radioactive species of interest. Each implant and decay event was tagged with an absolute time stamp. The half-lives of decaying species were deduced by taking the difference between the absolute time of a fragment implant and its subsequent beta decay. In addition, beta-delayed gamma rays were monitored by an array of three Ge clover detectors and two high purity Ge detectors that surrounded the implantation detector.

To deduce the decay properties of ^{58}V, a gate was defined in the energy loss versus TOF spectrum. A $T^{\beta}_{1/2} = 180(36)$ ms was extracted by fitting Fig. 2a with a one component exponential with background. A lifetime curve was also obtained by correlating ^{58}V fragments with beta-delayed gamma rays of energy 880 keV (see discussion below). Considering this half-life, $T^{\beta-\gamma}_{1/2} = 218(30)$ ms, along with $T^{\beta}_{1/2}$, an adopted half-life of 202(36) ms was obtained for the decay of ^{58}V. This half-life is consistent with previous measurements performed by Sorlin et al. [15], $T_{1/2} = 205(20)$ ms, and Ameil et al. [16], $T_{1/2} = 200(20)$ ms. In addition, a single peak was observed at 879.9(2) keV in the beta-delayed gamma ray spectrum below 1.5 MeV (see Fig. 2b). This result is in general agreement with the work of Sorlin et al. [15] who observed a broad peak at 900(100) keV in

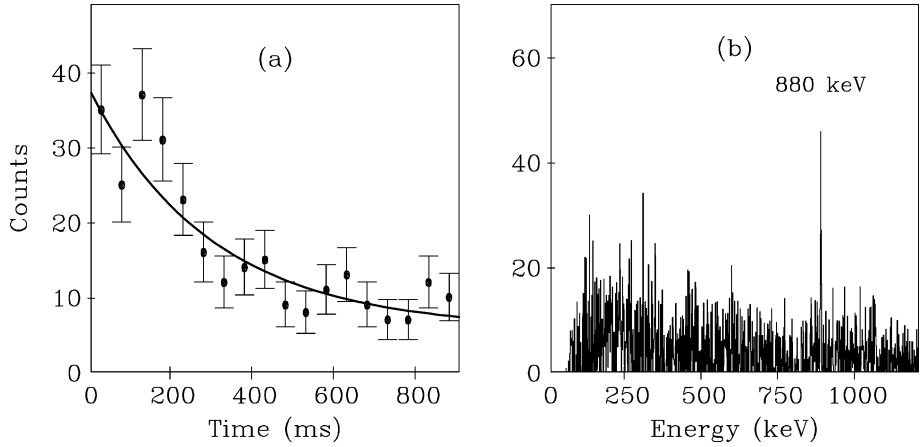

Fig. 2. (a) Lifetime curve following the correlation of ^{58}V implants and subsequent beta decays. (b) β-delayed gamma-ray spectrum following the decay of ^{58}V.

BGO scintillator detectors following the beta-delayed gamma emission of ^{58}V. This 900 keV transition had a FWHM approximately twice that of other transitions observed in their BGO detectors. The authors proposed this peak as a doublet, which may contain the $4^+ \rightarrow 2^+ \rightarrow 0^+$ cascade. However, no evidence for a second transition in the range 800–1000 keV, with similar intensity to the 880 keV gamma ray, was observed in the present study.

In general, the depopulation of excited states in even–even nuclei is characterized by a significant portion of the gamma ray intensity passing through the first excited 2^+ state. Thus the $2_1^+ \rightarrow 0_1^+$ transition should be the most intense. One exception, in some even–even nuclei, is the presence of a 3^- state at similar energy to the 2_1^+ state. However, the systematics of the lighter Cr isotopes do not support a low-energy 3_1^- in this mass region. Therefore, the 880 keV β-delayed gamma ray observed in the present study is proposed as the $2_1^+ \rightarrow 0_1^+$ transition in ^{58}Cr.

The low-energy level structures of the neutron-rich chromium isotopes in the range $N = 28$–36 are shown in Fig. 3, where the data was obtained from Refs. [4,14,17,18]. As compared to ^{54}Cr$_{30}$ and the new measurement for ^{58}Cr$_{34}$, there is a clear rise in $E(2_1^+)$ for ^{56}Cr$_{32}$. This peak in the $E(2_1^+)$ value for ^{56}Cr$_{32}$ provides empirical evidence for a significant subshell gap at $N = 32$.

Tu et al. [9] attributed the increase in binding at $N = 32$ for ^{52}Ca to the $Z = 20$ shell closure. However, based on the present measurement, a peak in $E(2_1^+)$ is now seen for ^{56}Cr$_{32}$, which resides in the middle of the $Z = 20$–28 shell. In addition, although $E(2_1^+)$ values increased at $N = 32$ for the calcium isotopes, this behavior is not observed for nickel (see Fig. 4, data taken from Refs. [4,14,17, 19]), which has a proton closed shell. If the strength of $N = 32$ were reinforced by a proton shell closure, a similar peak in $E(2_1^+)$ would be expected for ^{60}Ni. An alternative explanation for the appearance of the $N = 32$ subshell for neutron-rich systems is to consider a change in the proton–neutron monopole interaction strength. Nickel has a closed proton shell at $Z = 28$. According to Federman and Pittel [20], the proton–neutron interaction is strongest when the orbitals they occupy strongly overlap. The overlap between the proton and neutron orbitals is maximum

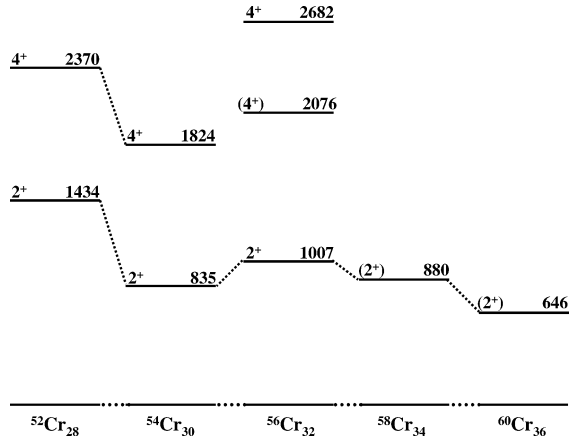

Fig. 3. Low-energy level scheme for neutron-rich chromium isotopes in the range $28 \leqslant N \leqslant 36$. The $E(2_1^+)$ values were obtained from Refs. [4,14,17,18].

when $\ell_n \approx \ell_p$ [20]. Therefore, when $Z = 28$, the $1f_{7/2}$ orbital is filled and the $\pi 1f_{7/2}$–$\nu 1f_{5/2}$ interaction should be strong, depressing the energy of the $\nu 1f_{5/2}$ orbital [21]. The $1f_{5/2}$ neutrons would act to stabilize the $1f_{7/2}$ proton configuration [22]. As protons are removed from the $1f_{7/2}$ orbital, the $\pi 1f_{7/2}$–$\nu 1f_{5/2}$ interaction weakens. When $Z = 20$, no protons occupy the $1f_{7/2}$ orbital in the ground state, thus the $\pi 1f_{7/2}$–$\nu 1f_{5/2}$ interaction should be diminished. This reduced monopole interaction, and the significant $2p_{1/2}$–$2p_{3/2}$ spin-orbit energy splitting, results in the emergence of the $N = 32$ subshell.

To probe the proton–neutron monopole interaction, ideally, the single-particle energies for the $2p_{3/2}$, $2p_{1/2}$ and the $1f_{5/2}$ orbital would be monitored. These energies may be deduced for the odd A, $N = 29$ isotones using spectroscopic factors extracted following transfer reactions. However, experimental information is limited. An example of such complications may be found in ^{53}Cr. A large spectroscopic factor has been extracted for a high-energy state at 3.63 MeV [23]. However, there is some uncertainty pertaining to the spin of this $\ell = 1$ state [23,24], which seriously impacts the ordering of the single-particle orbitals.

Due to the difficulty in extracting single-particle energies from experimental data for the $N = 29$ isotones, several authors have calculated these values. The single-particle energies for $2p_{3/2}$, $2p_{1/2}$ and $1f_{5/2}$ orbitals in the $N = 3$ shell for ^{57}Ni$_{29}$ have been

calculated by Trache et al. [25] and Duflo and Zuker [26]. Considering a ground state spin of 3/2 for ^{57}Ni [27], the lowest orbital in this shell would be $2p_{3/2}$. The $1f_{5/2}$ state was calculated at ≈ 1 MeV above $2p_{3/2}$, followed by $2p_{1/2}$. As protons are removed from $1f_{7/2}$, the single-particle energies for the $2p_{3/2}$, $2p_{1/2}$ and $1f_{5/2}$ orbitals shift. By ^{49}Ca$_{29}$, the $\nu 1f_{5/2}$ and the $\nu 2p_{1/2}$ orbitals have inverted [26].

For this study, shell-model calculations in the region $N = 28$–40 and $Z = 20$–28 were carried out in a *pf*-shell model space with an FPD6 effective interaction [28]. For the Ca isotopes the full basis calculation is feasible. The calculated energies of the lowest 2^+ states in the Ca isotopes are (in MeV) 3.66 (^{48}Ca), 1.33 (^{50}Ca), 2.75 (^{52}Ca), 1.47 (^{54}Ca), 1.37 (^{56}Ca) and 1.30 (^{58}Ca). The agreement with the experimental values in ^{48}Ca, ^{50}Ca and ^{52}Ca is good. The high energy of the 2^+ state in ^{48}Ca is due to a rather good $1f_{7/2}$ shell closure, and the relatively high energy for the 2^+ state in ^{52}Ca is due to a partial shell closure for the $2p_{3/2}$ shell. Beyond ^{52}Ca the effective single-particle energies of the $2p_{1/2}$ and $1f_{5/2}$ orbits are close and there are no other shell effects until the ^{60}Ca closed shell. In nuclides around ^{60}Ca the $1g_{9/2}$ orbit may become important but this is not included in the model space and there is no experimental information available.

For higher Z the shell-model calculation in the full *pf* shell quickly becomes intractable because of the large dimensions. In a few cases such as ^{56}Ni the Monte Carlo shell model has been used [29] (for which the FPD6 interaction still gives a good spectrum). However, the good closure of the $1f_{7/2}$ shell at ^{48}Ca means that to a good approximation the nuclei beyond $N = 28$ may be treated as neutrons in the ($2p_{3/2}$, $2p_{1/2}$, $1f_{5/2}$) model space. When this truncation is made for the Ca isotopes the energies of the 2^+ states (see Fig. 4) and their wave functions are close to those of the full space, which includes $1f_{7/2}$. (These truncated calculations use as inputs the single-particle levels in ^{49}Ca as obtained from FPD6 which are close to the experimental values.) For higher Z there is clear evidence of the dominance of the $1f_{7/2}$ shell for protons in the 0^+, 2^+, 4^+, 6^+ spectra of ^{50}Ti, ^{52}Cr and ^{54}Fe. ^{56}Ni shows a partial $1f_{7/2}$ shell closure (e.g., the relatively high 2^+ energy). Thus for protons the model space is truncated to the pure $1f_{7/2}$ shell with the proton two-body interaction taken as a function of Z to match exactly the 0^+, 2^+, 4^+, 6^+ spectra of ^{50}Ti, ^{52}Cr and ^{54}Fe. The neutron single-particle energies are linearly interpolated between ^{49}Ca and ^{57}Ni such that the spectrum of single-particle states in ^{57}Ni is reproduced. This defines the input to the shell-model interpretation of the 2^+ energies.

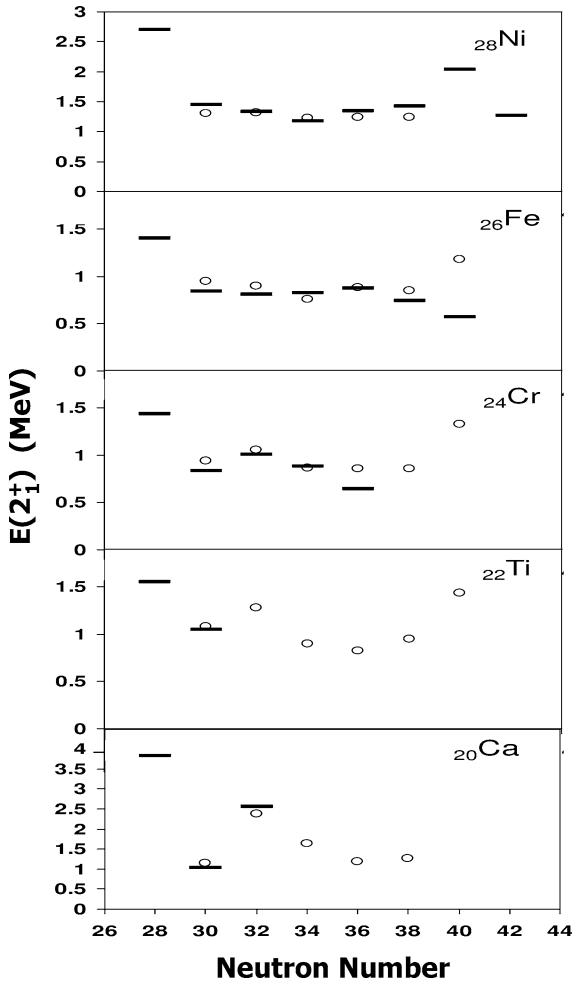

Fig. 4. $E(2_1^+)$ versus neutron number for neutron-rich nuclides between $20 \leqslant Z \leqslant 28$. The experimental $E(2_1^+)$ values are denoted by dashes, where the data was obtained from Refs. [4,14,17,19]. The open circles represent $E(2_1^+)$ values obtained from truncated shell-model calculations. See text for details.

Fig. 5 depicts the low-energy level structure for the odd A, $N = 29$ isotones within the vicinity $20 \leqslant Z \leqslant 28$, where data was taken from Ref. [4]. For comparison, the levels predicted via shell-model calculations for ^{49}Ca and ^{57}Ni are also shown. The energies of the

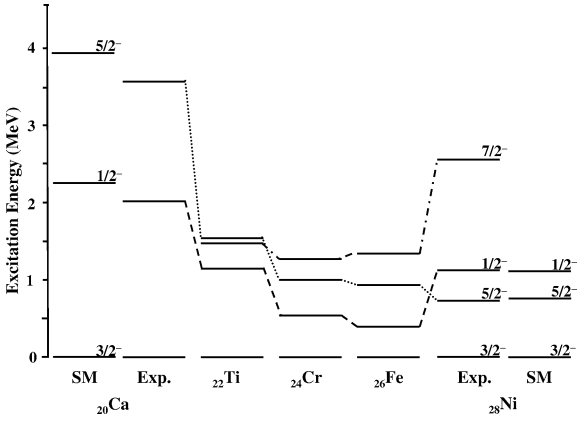

Fig. 5. Systematics of the low-energy states for the odd A $N = 29$ isotones in the range $20 \leqslant Z \leqslant 28$ [4]. Shell model results for ^{49}Ca and ^{57}Ni are also depicted.

$3/2^-$, $1/2^-$ and $5/2^-$ states follow the general behavior of the $\nu 2p_{3/2}$, $\nu 2p_{1/2}$ and $\nu 1f_{5/2}$ orbitals, respectively. At $Z = 20$, a substantial gap is observed between the $\nu(2p_{1/2}$–$1f_{5/2})$ and the $\nu(2p_{3/2}$–$2p_{1/2})$ orbitals. The existence of these gaps suggest an $N = 32$ and possibly an $N = 34$ subshell for calcium isotopes. As protons begin to fill the $1f_{7/2}$ orbital, the $5/2^-$ state is lowered. By Ni, the $\pi 1f_{7/2}$–$\nu 1f_{5/2}$ interaction is maximum and draws the $\nu 1f_{5/2}$ orbital below $\nu 2p_{1/2}$, which eliminates $N = 32$ subshell closure.

For chromium isotopes beyond $N = 32$, in addition to the present measurement, Sorlin et al. [17] observed the $2_1^+ \rightarrow 0_1^+$ transition of ^{60}Cr at 646 keV following the beta decay of ^{60}V. Considering the new $E(2_1^+)$ measurement for ^{58}Cr at 880 keV and Sorlin's measurement [17], a considerable decrease in $E(2_1^+)$ is observed beyond $N = 32$ for Cr (see Fig. 3). The overall $E(2_1^+)$ trends in neutron-rich chromium isotopes imply that as neutrons fill the $1f_{5/2}$ orbital, the $\pi 1f_{7/2}$–$\nu 1f_{5/2}$ quadrupole interaction strengthens, inducing nuclear deformation [20]. Such effects have been previously noted in, for example, the Mo isotopes, where a strong $\pi 1g_{9/2}$–$\nu 1g_{7/2}$ proton–neutron interaction produces deformed ground state structures beginning at ^{100}Mo [30]. The relatively low energy of the first excited 2^+ state of Cr, as compared with Fe, Zn and Ge isotopes (see Fig. 4), may be evidence of oblate-prolate shape coexistence predicted in this region [17]. However, based on shell-model calculations for chromium isotopes (see Fig. 4) the 2_1^+ energy level is predicted to remain fairly constant for $34 \leqslant N \leqslant 38$. Further studies in this mass region are necessary to better understand the low-energy structure of these Ca, Ti and Cr nuclides toward $N = 40$.

The decay properties of ^{58}Cr have been studied following the beta decay of ^{58}V. A beta-delayed gamma ray was observed at 879.9(2) keV and has been assigned to the $2_1^+ \rightarrow 0_1^+$ transition in ^{58}Cr. The even–even systematics of the neutron-rich chromium isotopes indicate an increase in $E(2_1^+)$ at $N = 32$. Following the present measurement, $E(2_1^+)$ for chromium isotopes were found to peak at $N = 32$. This rise in $E(2_1^+)$ is consistent with the increase observed at $N = 32$ for calcium isotopes. Although this trend does not continue beyond $Z = 24$, this may be due to the lowering of the $\nu 1f_{5/2}$ orbital as a result of a strong $\pi 1f_{7/2}$–$\nu 1f_{5/2}$ proton–neutron monopole interaction. The data is in agreement with shell-model calculations, which also show enhanced binding at $N = 32$ for $_{20}$Ca, $_{22}$Ti and $_{24}$Cr. It would be of interest to pursue $E(2_1^+)$ measurements for Ti and Ca isotopes beyond $N = 32$ to determine whether $N = 32$ is a good subshell closure for more neutron-rich nuclides.

Acknowledgements

This work was supported in part by the National Science Foundation under Grant Nos. PHY-9528844, PHY-0070911 and PHY-9970991. We thank the operations staff of the NSCL for the successful completion of these measurements. We acknowledge the ECR group at the NSCL for development of the ^{70}Zn primary beam and M. Steiner for identifying and tuning the secondary beam.

References

[1] M.G. Mayer, J.H.D. Jensen, Elementary Theory of Nuclear Shell Structure, Wiley, New York, 1955.
[2] L. Grodzins, Phys. Lett. 2 (1962) 88.
[3] F.S. Stephens et al., Phys. Rev. Lett. 29 (1972) 438.
[4] R.B. Firestone, Table of Isotopes, 8th edn., Vol. 1, Wiley, New York, 1996.
[5] M. Górska et al., Phys. Rev. Lett. 79 (1997) 2915.
[6] G. Sadler et al., Nucl. Phys. A 252 (1975) 365.
[7] F. Tondeur, Nuclei far from stability 4, Helsingor, CERN Report 81-09 (1981) 81.

[8] A. Huck et al., Phys. Rev. C 31 (1985) 2226.
[9] X.L. Tu et al., Z. Phys. A 337 (1990) 361.
[10] W.A. Richter, M.G. Van der Merwe, B.A. Brown, Nucl. Phys. A 586 (1995) 445.
[11] B.A. Brown, W.A. Richter, Phys. Rev. C 58 (1998) 2099.
[12] R. Chapman, S. Hinds, A.E. Macgregor, Nucl. Phys. A 119 (1968) 305.
[13] T.T. Bardin et al., Phys. Rev. C 14 (1976) 1782.
[14] J.I. Prisciandaro et al., Nucl. Phys. A 682 (2001) 200c.
[15] O. Sorlin et al., Nucl. Phys. A 632 (1998) 205.
[16] F. Ameil et al., Eur. Phys. J. A 1 (1998) 275.
[17] O. Sorlin et al., Nucl. Phys. A 669 (2000) 351.
[18] A.M. Nathan et al., Phys. Rev. C 16 (1977) 192.
[19] M. Hannawald et al., Phys. Rev. Lett. 82 (1999) 1391.
[20] P. Federman, S. Pittel, Phys. Lett. 69B (1977) 385.
[21] G. Cata et al., Z. Phys. A 335 (1990) 271.
[22] A. De-Shalit, M. Goldhaber, Phys. Rev. 92 (1953) 1211.
[23] M.N. Rao et al., Nucl. Phys. A 121 (1968) 1.
[24] J. Kopecký, K. Abrahams, F. Stecher-Rasmussen, Nucl. Phys. A 188 (1972) 535.
[25] L. Trache et al., Phys. Rev. C 54 (1996) 2361.
[26] J. Duflo, A.P. Zuker, Phys. Rev. C 59 (1999) R2347.
[27] M.R. Bhat, Nucl. Data Sheets 85 (1998) 415.
[28] W.A. Richter et al., Nucl. Phys. A 523 (1991) 325.
[29] T. Mizusaki et al., Phys. Rev. C 59 (1999) R1846.
[30] P.F. Mantica et al., Phys. Rev. C 63 (2001) 034312.